OPTOELECTRONICS AND ADVANCED MATERIALS – RAPID COMMUNICATIONS Vol. 1, No. 5, May 2007 p. 252 - 260

Effect of precursor molarity on physical properties of In_2O_3 films

P. PRATHAP, Y. P. V. SUBBAIAH, K. T. RAMAKRISHNA REDDY*
Thin Film Laboratory, Department of Physics, Sri Venkateswara University, Tirupati – 517 502, India

In_2O_3 thin films have been deposited on glass substrates by spray pyrolysis using $InCl_3$ as the precursor. The effect of precursor concentration that varied in the range, 0.01-0.25 M on the physical properties of sprayed In_2O_3 films deposited at 400 ^oC was investigated. The structural properties of the as-deposited films were studied using X-ray diffractometer and Atomic force microscope. The XRD analysis indicated that the layers had cubic structure with (222)/(400) as the preferred orientation. The AFM studies revealed a decrease of grain size at higher precursor concentrations with an increase of surface roughness. The layers were optically characterized in order to evaluate the absorption coefficient, optical band gap, refractive index, extinction coefficient and other optical parameters. An average visible transmittance of ~ 90 % was observed with an optical band gap of 3.62 eV for the layers grown at a solution concentration of 0.1 M. The Hall effect measurements revealed that the films deposited at a solution concentration, 0.1 M exhibit a minimum resistivity of $2.72x10^{-3}$ Ωcm with the carrier concentration and mobility of the order of $7.6x10^{19}$ cm^{-3} and 30.2 cm^2/Vs respectively. The layers showed the highest figure of merit of $8.2x10^{-3}$ Ω^{-1}.

(Received December 11, 2006; accepted April 5, 2007)

Keywords: In_2O_3 films, Spray pyrolysis, Optical parameters

1. Introduction

Thin films of transparent conducting oxides (TCOs) have been widely used as transparent electrodes in solar cells, panel liquid crystal displays and organic light emitting diodes [1] because of their unique properties of high optical transparency in visible region and high conductivity, which can be modulated from insulator to metal. In general, the electrical conductivity in any semiconductor can be improved by increasing the charge carrier concentration or the carrier mobility. However, an increase in the charge carrier concentration will decrease the optical transparency due to the free carrier absorption. An increase of the carrier mobility can improve the conductivity with out sacrificing optical transparency. Hence, the materials with high carrier mobility would enhance the overall properties of TCO materials [2]. The conductivity of TCOs is a function of number of oxygen vacancies present in the matrix, each of which donate two electrons to the conduction band and dopant concentration. Various binary, ternary and compound oxide materials have been developed and obtained good opto-electronic transport properties. The use of multi-component oxide materials makes it possible to design TCO films suitable for specialized applications, as their physical properties can be precisely controlled by changing the chemical composition or by doping. But the preparation of doped ternary and multi-component oxide layers with suitable composition and understanding of the chemistry involved are rather difficult when compared to undoped TCO materials. In general, undoped binary oxide films are insulators in its stoichiometric condition. But the conductivity of pure oxide layers can be improved to the level of doped layers by suitably controlling the density of oxygen vacancies, each of which donate two electrons to the conduction band and can be tailored from insulator to conductor. This deficiency determines the conductivity of undoped oxide layers. Thus the binary TCOs are mainly oxygen deficient and the ultimate attainable properties of TCOs are material dependent [3].

Various undoped metal oxides such as ZnO, SnO_2, CdO, Sb_2O_5 and doped metal oxides like In_2O_3: Sn, ZnO: Al, CdO: Sn and ternary compounds such as $Cd_2In_2O_4$, $Zn_2In_2O_5$, have been used in industrial applications depending on their suitability. Among the different metal oxides, In_2O_3 was found to be a potential material that has wide band gap, low resistivity and highly stable when it is exposed to different atmospheres at higher temperatures (~ 1000 ^oC) [4,5]. Thin films of In_2O_3 can be prepared by a variety of physical and chemical methods. In the present study, In_2O_3 films were prepared by spray pyrolysis technique.

Spray pyrolysis is a versatile and effective technique used to deposit metal oxide thin films over large areas on large scale for various industrial applications. Recent advances in spray pyrolytic deposition process makes possible for the preparation of metal oxide, chalcogenide and even metal films [6-10]. Spray pyrolysis opens up the possibility to control the film morphology and particle size in the nanometer range. The quality and properties of the films depend largely on the process parameters. The most important parameter for film formation is the substrate surface temperature. At higher substrate temperatures, the films will become rough and exhibit a more porous microstructure. If the temperature is too low, the films are cracked and mostly amorphous in nature. In addition, precursor solution and other additives in the precursor can also influence the morphology, crystallinity, texture and

other physical properties of the deposited films. The primary requirement to obtain good quality thin films is the better control over the deposition parameters. This technique offers an easy control over the deposition conditions such as substrate temperature, rate of deposition, concentration of precursor solution etc. In these process parameters, the most critical one is the size of droplet and their distribution over the preheated substrates. The enhancement in deposition efficiency results in the formation of good quality thin films. The properties of films can be easily tailored by controlling the process conditions. As the electro-optical properties of thin films are highly sensitive to microstructure as well as the level of residual stress/strain caused during the deposition process [11] and orientational changes which inturn depend on the deposition conditions [12], it is essential to study the influence of each process parameter on the physical properties of the grown films. Although there are reports in the literature on the growth of sprayed In_2O_3 films, the data available on the influence of solution concentration on different physical parameters are very meagre. Hence, in the present investigation, it was aimed to study the influence of solution concentration, (S_c) on the physical properties of undoped indium oxide (In_2O_3) films that includes preferred orientation, grain size, lattice strain, energy band gap, refractive index, charge carrier density etc.

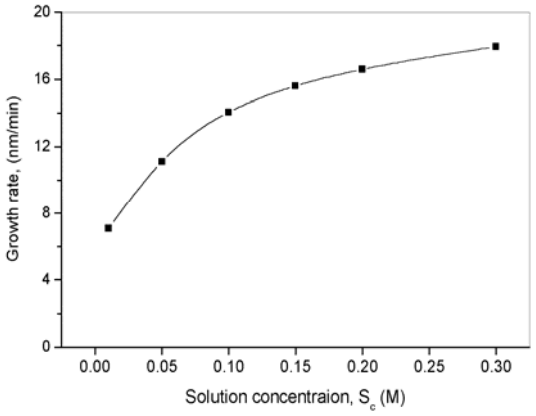

Fig. 1. The variation of the growth rate of as a function of solution concentration.

2. Experimental details

Thin films of In_2O_3 were prepared using chemical spray pyrolysis. Resistively heated coil was employed to provide thermal energy necessary for the pyrolytic process. The upper side of the resistance coil was covered with a thick copper plate and the other sides were thermally insulated from the atmosphere in order to reduce the loss of heat energy. The Eurotherm temperature controller was used to maintain the pre-determined substrate temperature using a Chromel-Alumel thermocouple as a temperature sensor for the controller. Stainless steel (Model 1/4 JAU-SS) spray gun was used to spray the precursor solution, which was suspended from a rigid support. This consists of two inlet tubes, one of which is connected to solution reservoir and the other to a gas compressor. The gas pressure and flow rate can be monitored through the flow meter set-up. The spray head was moved in the horizontal plane by means of a microprocessor controlled stepper motor system in order to get uniform films on the substrate. High purity (5N) $InCl_4$ was dissolved in de-ionized water to prepare the precursor solution at different concentrations in the range, 0.01 - 0.25 M. Compressed purified air was used as the carrier gas at a pre-determined flow rate of 8 l/min and the solution was sprayed at a flow rate of 6 ml/min onto ultrasonically cleaned corning 7059 glass substrates. The optimum substrate temperature was determined as 400 ± 5 ^oC in our previous studies reported elsewhere [13] and the same is maintained in this study. The substrate to nozzle distance was maintained as 25 cm. In the spray pyrolysis, the temperature of the substrates decreases due to the interaction of sprayed droplets of the solution with the pre-heated substrate. Hence, the precursor solution was sprayed onto the substrates at an interval of 1-2 min. i.e., the spray process lasts for 10 sec and was paused for 1-2 min, in order to recover the required substrate temperature and for ensuring the complete re-evaporation of the reaction by products. Such type of spraying cycles was repeated several times and after completion of the deposition process the films were allowed to cool slowly to room temperature. The structural surface topological and morphological studies of the films were carried out using Siemens X-ray diffractometer, Hitachi scanning electron microscope and Vecco atomic microscope. The electrical properties of the films were carried out using Hall effect measurements using van der Pauw method. The optical properties were evaluated using Hitachi UV-Vis-NIR spectrophotometer with unpolarised light.

3. Results and discussion

The visual appearance of all the grown layers grown at different solution concentrations (S_c) indicated that the layers were homogeneous, pinhole free and well adherent to the substrate surface. The layers grown at $S_c < 0.15$ M were transparent where as the layers grown at $S_c > 0.15$ M were whitish in appearance.

3.1. Structural properties

Fig. 1 shows the growth rate of In_2O_3 films as a function of concentration of the spraying solution, S_c. The growth rate was calculated from the ratio of thickness of the films and deposition time, and found to have a linear dependence on the S_c between 0.01 M and 0.1 M, whereas an exponential increase was observed above 0.15 M. The initial monotonous increase in the growth rate with the molarity can be understood from the fact that the oxide films can be grown by a continuous adsorption followed by reaction of metal containing species with the adsorbed water molecules [14]. Hence, the growth rate of In_2O_3 mainly depends on the number of indium species available to form the corresponding layer. The initial linear increase in the growth rate upto $S_c \sim 0.1$ M can be attributed to the

appropriate proportion of indium containing species and oxygen from water molecule. At higher S_c (> 0.1 M) values, as the concentration of indium species is very high and the available oxygen from the water molecule may be insufficient to form the desired film that caused to decrease the growth rate of the films with a deviation from the linearity. Fig. 2 shows the X-ray diffraction profiles of In_2O_3 films deposited at a temperature of 400 ^oC with different precursor concentrations, S_c. All the grown layers were polycrystalline with a strong (222) and (400) reflection and weak (211), (400), (411), (440) and (622) reflections. From this data, it can be observed that the preferred orientation of the grains varied with the variation of the precursor solution. The films deposited at $S_c \sim 0.01$ M showed a low intensity for the (222) reflection, which was increased for $S_c \sim 0.1$ M. This showed an improvement in the crystallinity of the as grown films at $S_c \sim 0.1$ M in the (222) orientation. Further increase in the S_c value led to a change in the film orientation from (222) to (400). The films grown at 0.25 M exhibited multi-phase orientation with (222) and (400) as dominant peaks. This clearly indicates the influence of solution concentration on the preferred orientation of grains in the films. Agashe et al. observed a similar behaviour of change in the growth direction of SnO_2 films prepared by spray pyrolysis and reported that with the increase of S_c, tin occupies the regular lattice sites at low concentrations. When the S_c value of the precursor solution increases certain limit, Sn occupies interstitial sites rather than lattice vacancies, which change the preferred growth of the films. Hence, the present results correlated well with the reported observations and the behaviour of preferred orientation can be attributed to the theory given by Agashe et al. [15]. Elangovan et al. observed a similar behaviour for spray deposited SnO_2: F films prepared at different precursor concentrations and explained the variation of preferred orientation due to the variations in the precursor concentration that alter the nucleation and growth process, which decides the orientation of the film [16]. Moreover, the change in the preferred orientation can be explained that the orientation of grains in a particular direction depends on both the deposition rate and substrate temperature [17]. In this study, as the substrate temperature was kept constant at 400 ^oC, the parameter influencing the film growth direction and its characteristics was the deposition rate, which is directly related to the number of indium containing species supplied in the solution onto the substrate surface. At higher S_c values as the deposition rate was very high i.e., number of indium containing species in the precursor solution increased with the increase of precursor concentration, which resulted in the formation of In_2O_3 films containing small grains with less pronounced preferred orientation, and the available time for grain growth is short due to which the (222) orientation did not sustain itself. This results in the dominance of random orientation over the (222) direction observed at higher S_c values. Mouthino et al. [18] reported that the lack of preferential orientation is due to the increase of film thickness. From this study, it can be ascertained that it is easy to control the growth rate of the films and interstitial incorporation of constituent atoms, which influence the properties of the films. The earlier reports showed that in case of the films prepared using evaporation methods in oxygen atmosphere, the preferred orientation is mainly dependent on the level of oxygen present in the crystal structure [19]. But in case of the films prepared by chemical methods, most of the authors reported the prevalence of (222) orientation [20,21]. Moreover, epitaxially grown indium oxide films using electron beam evaporation method also showed the existence of (222) orientation [22].

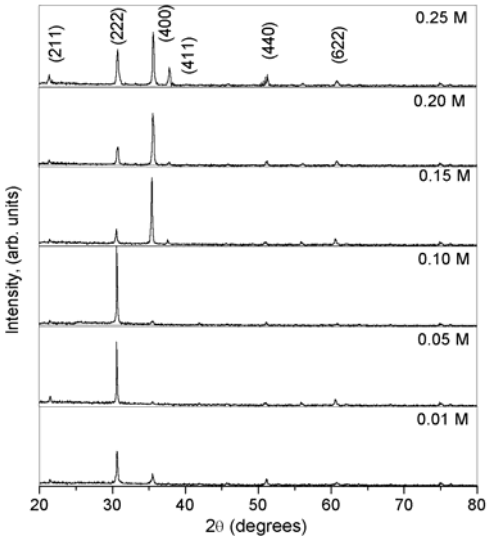

Fig. 2. X-ray diffraction patterns of indium oxide films grown on glass substrates at T_s = 400 ^oC.

The grain size (D) of In_2O_3 films prepared at different S_c values was calculated from the fringe width at half maximum (FWHM) of the (222) peak using Scherrer formula [23],

$$D = \frac{0.9\lambda}{\beta_{2\theta}\cos\theta} \quad (1)$$

where β is the FWHM and λ is the wavelength of CuK_α radiation (1.542 Å). Table 1 shows the variation of grain size of In_2O_3 films deposited as a function of S_c. The grain size was high at $S_c \sim 0.1$ M and reduced with further increase in the S_c. This reduction in the grain size at higher S_c may be due to the re-orientation of the films that is responsible for the formation of smaller grains with less pronounced preferred orientation. Moreover, the deposition rate is very high at higher S_c and can also influence the growth kinetics of the grains [24].

Fig. 3 shows the three dimensional AFM images of In_2O_3 films scanned over an area of $2\mu m$ x $2\mu m$. It can seen that the surface morphology of the films was highly influenced by precursor solution concentration, S_c. All the pictures showed spherical grains that were uniformly distributed irrespective of the S_c. The surface roughness was found to decrease from 20 nm to 16 nm when the S_c varied from 0.01 M to 0.1 M. This decrease in the surface

roughness might be due to the coalescence of small grains. When the S_c > 0.1 M, roughness of the films increased drastically to 28 nm at S_c = 0.25 M despite a decrease in the grain size of the films. This might be due to the increase of rate of deposition with the increase of solution concentration as discussed above.

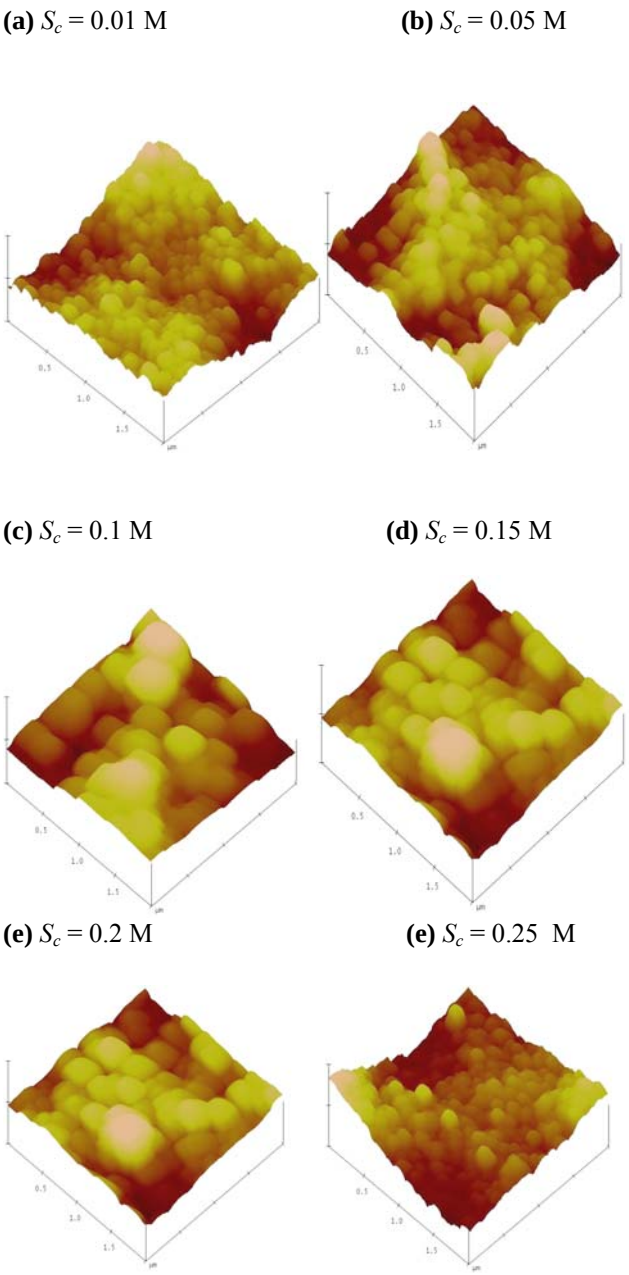

Fig. 3. AFM pictures of the sprayed In_2O_3 films prepared at six solution concentrations.

The lattice parameter 'a' for cubic In_2O_3 films was calculated using the relation,

$$a = d\,(h^2+k^2+l^2)^{1/2} \tag{2}$$

where, h, k, l are the lattice planes and 'd' is the interplanar spacing, measured using Bragg's equation. Fig. 4 shows the variation of lattice constant with S_c. The lattice constant of In_2O_3 films was found to be lower than the reported value of 10.118 Å [25] for the cubic In_2O_3. The lattice constant increased from 9.951 Å to 9.965 Å as the molarity of the precursor was increased. This implied that the thicker films exhibit less defects [26].

The lattice distortion ($\Delta d/d_{hkl}$) is defined as,

$$\Delta d/d_{hkl} = (d_{exp} - d_{hkl})/d_{hkl} \tag{3}$$

where d_{exp} is the interplanar spacing determined from the position of the experimental peak by using Bragg formula, and d_{hkl} is the theoretical value calculated from the lattice constant (10.118 Å). As the statistical microstrain, $\varepsilon = \Delta d/d_{hkl}$ in the films is proportional to lattice distortion, it is correlated with the XRD line broadening $\Delta(2\theta)$, which is caused due to the inhomogeneous strain as, [27]

$$\Delta(2\theta) = (2\tan\theta)\varepsilon$$

Generally, the strain in thin films arises from a number of sources such as departure from ideal stoichiometry and mechanical residual stress and the difference in the thermal expansion coefficients of the deposited film and substrate. Fig. 4 shows the variation of internal strain with solution concentration, which indicated a lowest microstrain for the films prepared at S_c ~ 0.05 M and increased beyond this value of molarity. This increase in the strain at higher S_c value could be due to the increase of film thickness or the rate of deposition. Korotcenkov et al. observed a similar behaviour for indium oxide films prepared by spray pyrolysis at higher precursor concentrations [28].

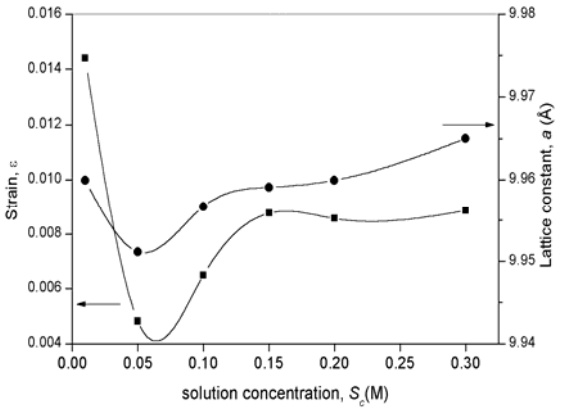

Fig. 4. Variation of strain and lattice constant with solution concentration.

The analysis of XRD data for preferred orientation in In_2O_3 films, prepared at different solution concentrations was carried out by

$$\text{Lotgering factor, } L = \frac{P_{(hkl)} - P_{(powder)}(hkl)}{1 - P_{(powder)}(hkl)} \tag{5}$$

where, $P_{(hkl)}$ is the ratio of the integrated XRD intensities of certain orientation (hkl) to the sum of all reflections and $P_{(powder)}(hkl)$ is the equivalent ratio for a randomly oriented powder sample [29]. The Lotgering factor, L reveals how strong a surface orientation (hkl) occurs with

respect to its powder sample. Negative values of $L(hkl)$ indicate a reduced occurrence of a certain orientation whereas the positive values of $L(hkl)$ indicate that the orientation (hkl) is strongly pronounced compared to the powder sample. From Fig. 5, the Lotgering factor for a powder sample with no preferred orientation would lie on the dashed line $L = 0$. The L value for (222) plane was found to approach unity at S_c ~0.1 M, indicating that this orientation was energetically preferred. Whereas, L was negative for (622) and (400) planes at $S_c > 0.15$ M, which indicated that these orientations were less pronounced. From this, it could be assumed that the decrease in the crystalline texture with the increase of solution concentration is caused by the increase in the rate of deposition that induces a more random growth pattern of the grains in the films [30].

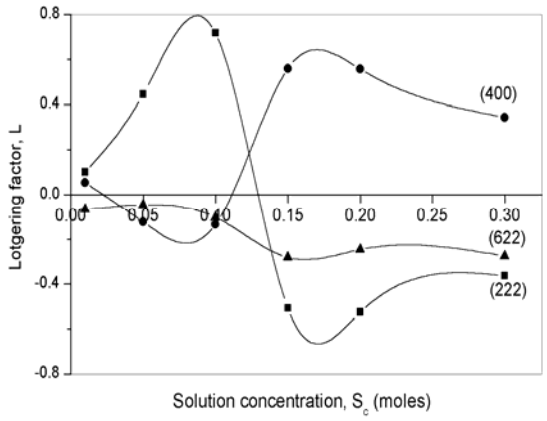

Fig. 5. Variation of Lotgering factor of different orientations in the films prepared at different solution concentrations.

3.2. Optical properties

The transmittance spectra of In_2O_3 films measured in the wavelengths between 300 nm and 1700 nm deposited for six different concentrations in the range, 0.01 M – 0.25 M is shown in Fig. 6. All the films showed good transmittance in the visible region and exhibited interference pattern, which implies that the films were highly uniform. The spectra showed a high transmittance, ~ 90 % for the films deposited at a concentration, S_c of 0.1 M and decreased with the increase of S_c due to the thickness effect, causing an increased absorption [31]. The higher transmittance observed in the films was attributed to less scattering effects, structural homogeneity and better crystallinity whereas the observed low transmittance in the layers might be due to the less crystallinity leading to more light scattering [32]. As the film thickness decreases, the absorption edge is shifted towards shorter wavelengths. Further, the shift in the fundamental absorption edge with the increase of solution concentration is nominal.

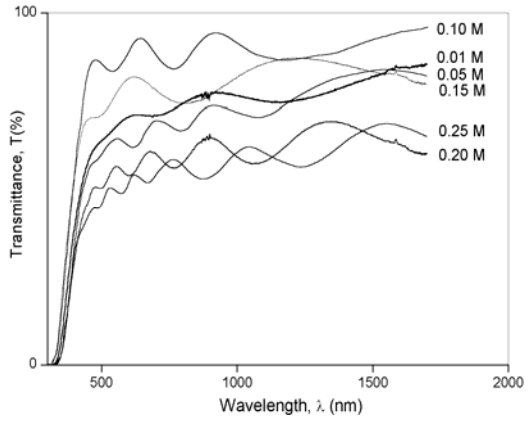

Fig. 6. Transmittance versus wavelength spectra of indium oxide films for different solution molarities.

The absorption coefficient, α in the strong absorption region where the envelop method is not valid as the region was interference free, was evaluated from the optical transmittance data using Lambert's principle,

$$\alpha = -(1/t) \ln T, \tag{6}$$

where T is the transmittance and 't' is the thickness of the film. In the lower absorption region of the interference zone, the absorption coefficient can be calculated using the relation [33],

$$\alpha = -\frac{1}{d}\left\{\ln\left[\frac{E_M - \left[E_M^2 - (n^2-1)^3(n^2-s^4)\right]^{\frac{1}{2}}}{(n-1)^3(n-s^2)}\right]\right\} \tag{7}$$

where $E_M = \dfrac{8n^2 s}{T_M} + (n^2-1)(n^2-s^2)$. Here n is refractive index of the film and s is the refractive index of the substrate.

The absorption coefficient at the absorption edge was determined to be of the order of 10^5 cm^{-1}. This high absorption in the films reflects the direct band to band transition [34]. Fig. 7 shows the spectral dependence of absorption coefficient in In_2O_3 films. In amorphous or polycrystalline materials the absorption coefficient follows exponential behaviour near the fundamental absorption edge that arises due to potential fluctuations of the internal fields associated with the structural disorder and is of the form [35],

$$\alpha = \alpha_\circ \exp\left[\frac{h\nu - E_1}{E_o}\right] \tag{8}$$

where α_o is a constant, h is the Plank's constant and E_o is width of the tail (Urbach tail) of the localized states in the forbidden band gap. The width of the tail is a direct measure of structural disorder [36]. The absorption coefficient as a function of the incident photon energy near the band edge was determined for all the films prepared with different precursor concentrations. From this data, the empirical parameter E_o was calculated from the plot of $\ln\alpha$ versus $h\nu$ as shown in Fig. 7, and the results are shown in Table. 1. The value of E_o was low for the films prepared at $S_c \leq 0.1$ M after which the variation in E_o was very less.

This represents the better crystallinity/structural order of the films prepared at S_c = 0.10 M. From this study, it was observed that the films with single orientation had less Urbach tail width that indicated better structural order in the films deposited at S_c ~ 0.1 M. The evaluated values of E_o are in close agreement with the reported data for sprayed indium oxide films [37].

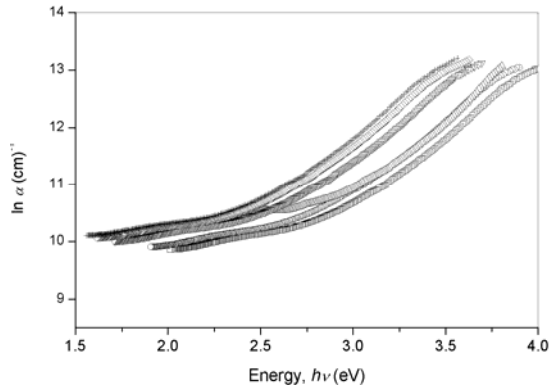

Fig. 7. Variation of absorption coefficient as a function of photon energy.

The electronic transition between the valence and conduction bands can either be direct or indirect. In the two cases, the transition of electron from the valence band to conduction band can be allowed or forbidden where such probability could not exist according to the transition probability, p. The transition probability follows the relation, which relates the energy band gap of the films and the absorption coefficient, α as a function of photon energy, $h\nu$,

$$(\alpha h\nu)^p = A\,(h\nu - E_g) \quad (9)$$

where A is a constant, E_g is the optical energy band gap. The nature of transition can be determined by plotting $(\alpha h\nu)^p$ against photon energy. For a suitable value of p, strain line behaviour of the plot can be obtained and extrapolation of which on to the energy axis gives the value of the energy band gap of the material. The value of p = *2* and *3* represents the direct allowed and direct forbidden transitions respectively. Further, the value of *p=1/2* and *1/3* represents the indirect allowed and indirect forbidden transitions respectively. In the present study, the variation of absorption coefficient with photon energy followed the above relation for *p=2*, indicating that the transition must correspond to a directly allowed electronic transition. Fig. 8 shows a plot of $(\alpha h\nu)^2$ versus $h\nu$ and the variation of energy band gap in the films deposited for five different solution concentrations. The energy band gap varied from 3.67 eV to 3.31 eV when the films deposited in the solution concentration range, 0.01M≤ S_c≤ 0.25M. The observed higher value of the energy band gap over the bulk value for the films deposited at lower precursor concentration might be due to the smaller crystallite size of the films. This could be explained on the basis of three-dimensional quantum size effect, which leads to an increase in the band gap with the decrease of crystallite size [38]. This is the usual phenomenon observed in the case of nanocrystalline materials. The decrease in the band gap at higher precursor concentrations, i.e., S_c≥0.1M, in spite of the decrease of crystallite size might be attributed to presence of high density of grain boundaries and disorders at the grain boundaries [39]. This was also supported from the variation of Urbach tail width.

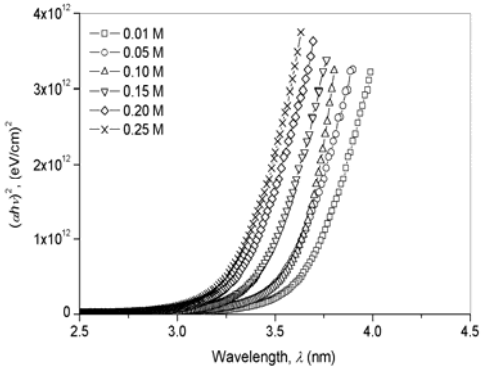

Fig. 8. $(\alpha h\nu)^2$ versus $h\nu$ plot of In_2O_3 films.

Table. 1. Grain size, energy band gap and width of the Urbach tail in In_2O_3 films.

S_c (M)	Grain size (nm)	Energy band gap, E_g (eV)	Width of the Urbach tail (meV)
0.01	53	3.67	331
0.05	82	3.61	301
0.10	91	3.59	286
0.15	65	3.41	308
0.20	57	3.34	335
0.25	54	3.31	352

The refractive index of the films was calculated from the transmittance versus wavelength spectrum. This method is based on the analysis of the transmittance spectrum of a weakly absorbing film deposited on a non-absorbing substrate [33]. The refractive index, n over the spectral range is calculated by using the envelopes that are fitted to the measured extreme. The refractive index, n is given by

$$n^2 = N + (N^2 - n_a^2 . n_s^2)^{1/2} \quad (10)$$

where $N = (n_a^2 + n_s^2/2) + 2\,n_a n_s T$

Here n_a and n_s are the refractive indices of air and substrate and $T = (T_{max} - T_{min})/ T_{max}.T_{min}$. T_{max} is the maximum envelope, and T_{min} is the minimum envelope. The refractive index 'n_f' of the films was found to decrease continuously with the increase of wavelength. The n values were in close agreement with the reported data for pulsed laser deposited indium oxide films [40]. The refractive index values obtained in the weak absorption region was fitted to the classical Cauchy relation,

$$n = a + \frac{b}{\lambda^2}, \quad (11)$$

where a and b are the Cauchy parameters and λ is the wavelength of the light used. The data followed the general relation given by Equation. (6) and the resultant equations were shown in the Table. 2 for all the films deposited at S_c values in the range, 0.01 – 0.25 M. This implied that the films had normal dispersion for the entire range of wavelength studied. Fig. 9 shows the variation of refractive index with wavelength where the solid curve represents the Cauchy fit. At higher wavelengths when $\lambda \to \infty$, the Cauchy's parameter, α represents the longer wavelength limit of refractive index, n_∞. It can be noted from Table. 2 that the refractive index increased with the increase of precursor concentration. This might be due to the increase in the density of the film [41]. As the thickness of the films increased with the increase of S_c, a reduction in the density of voids occur that could also cause an increase in the refractive index. Thus, by monitoring the refractive index of the films, it is possible to estimate the density of the films [42].

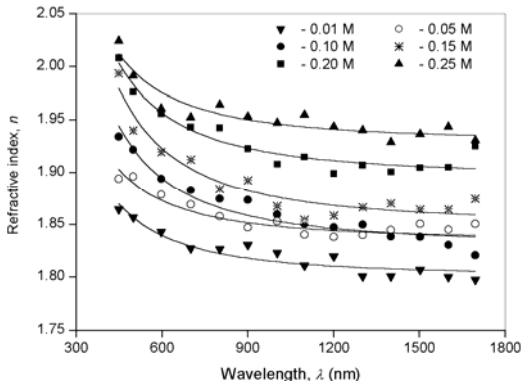

Fig. 9. Dispersion of refractive index and the corresponding Cauchy fit.

Table. 2. Cauchy fitting equations.

S_c (M)	Cauchy equations, $n =$
0.01	$1.80+1.40\text{x}10^4/\lambda^2$
0.05	$1.83+1.38\text{x}10^4/\lambda^2$
0.10	$1.80+2.30\text{x}10^4/\lambda^2$
0.15	$1.85+2.61\text{x}10^4/\lambda^2$
0.20	$1.89+2.16\text{x}10^4/\lambda^2$
0.25	$1.93+1.67\text{x}10^4/\lambda^2$

The extinction coefficient (k) was directly calculated from the absorption coefficient by using the relation [43],

$$k = \frac{\alpha\lambda}{4\pi} \quad (12)$$

The variation of extinction coefficient with wavelength is shown in Fig. 10. The evaluated value of extinction coefficient had a maximum at the fundamental absorption edge and its variation with wavelength was marginal. The extinction coefficient was low for the films prepared at S_c = 0.01 M and its value increases with the increase of S_c. This might be due to the increase in the thickness of the films with the solution concentration, which is the fundamental property of solids. The higher value of extinction coefficient at higher thicknesses could also be attributed to more light scattering in the films. However, the value of extinction coefficient was found to be high for all the films that may be due to the crystallographic defects such as grain boundaries and voids present in the layers.

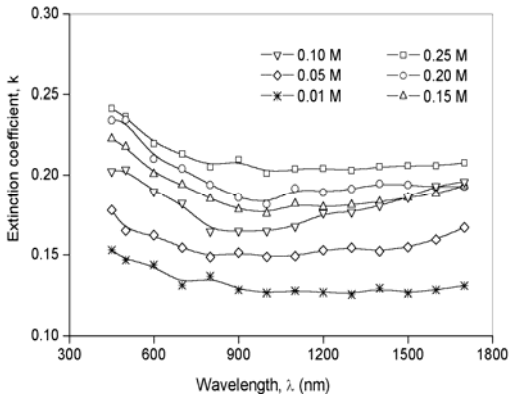

Fig. 10. Extinction coefficient as a function of wavelength.

3.3. Electrical properties

Fig. 11 shows the variation of carrier concentration (n), mobility (μ) and electrical resistivity (ρ) plotted against solution concentration, S_c. For the films prepared at S_c = 0.10 M, the carrier density was approximately 3.4×10^{19} cm^{-3} with an electrical resistivity of 8.92×10^{-3} Ωcm. The value of n increased to 7.6×10^{19} cm^{-3} with $\rho = 2.72\times10^{-3}$ Ωcm and approximately remains stable for S_c values between 0.15 M and 0.25 M. A modest mobility of < 30.2 cm^2/Vs was measured in all the films. The resistivity was low for the films prepared at S_c = 0.1M that shows the better crystallinity. The resistivity and mobility of the films prepared in the present study is close to the values observed for indium oxide films grown by pulsed laser deposition [5]. Further, the present study demonstrated low mobility for the films grown at higher concentration of the precursor. A sharp decrease in the value of μ at higher S_c values could be due to interstitially incorporated indium, which caused to change in the preferred orientation from (222) to (400). This also causes a reduction in the grain size and the existence of additional orientations other than (400), which may be responsible for the observed low mobility [44]. Moreover, as the films were prepared in the atmospheric ambience, additional incorporation of oxygen and other impurities cannot be minimized and therefore the transport properties of the films will be more affected. A continuous increase in the carrier concentration with the increase of S_c may be resulted from the interstitial indium atoms, which act as charge carrier donors to the conduction band. But the

interstitially incorporated indium atoms had a negative influence on the mobility and conductivity. In spite of a significant increase in the carrier concentration, the resistivity is decreased due to the decrease in the mobility at higher precursor concentrations. Finally, the prevalence of (222) orientation offers better properties than the (400) orientation in In_2O_3 films prepared by spray pyrolysis.

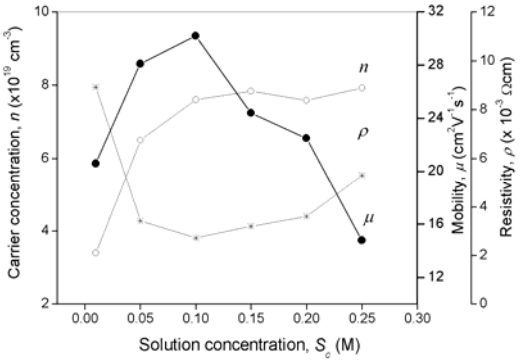

Fig. 11. Variation of carrier concentration, mobility, and resistivity with the solution concentration

The quality of transparent conducting films is best represented using the figure of merit (Φ), calculated from the transmittance and sheet resistance data. The higher values of the figure of merit represent the better performance of the transparent conducting film. The electrical conductivity and transmittance of TCO film should be as high as possible for application in solar cells. The figure of merit, proposed by Haacke, compares the performance of various transparent conductors [45] is given by

$$\varphi = T^{10} / R_s \qquad (13)$$

where T is the transmittance, R_s is the sheet resistance. As shown in Fig. 12 the best performance was obtained for the films prepared at S_c = 0.1 M which had Φ=8.2×10^{-3} Ω^{-1}, with a low electrical resistivity.

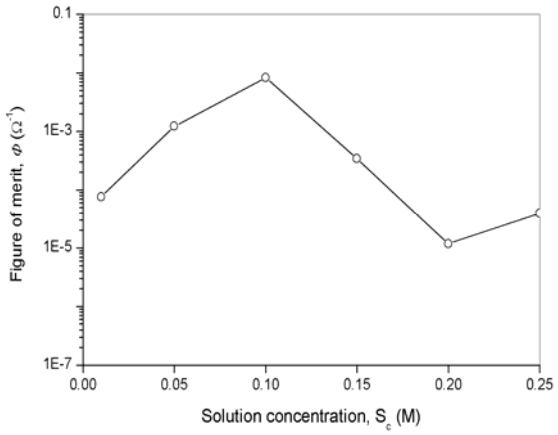

Fig. 12. Variation of figure of merit with the solution concentration.

4. Conclusions

In the present investigation, transparent and conducting indium oxide thin films have been synthesized systematically by chemical spray pyrolysis at different precursor solution concentrations (S_c), 0.01 – 0.25 M using predetermined deposition parameters such as substrate temperature, solution and gas flow rates. The growth rate of the films increased linearly with the increase of S_c upto 0.1 M above which the growth rate was non-linear. All the films deposited at a temperature, 400 ^oC for different precursor concentrations, S_c showed polycrystalline structure. The X-ray diffraction profiles of the as-deposited films showed a strong (222) and (400) reflection and a weak (211), (400), (411), (440) and (622) reflections. It was observed that the preferred orientation of the films was found to vary with the precursor concentration. But the films prepared at S_c ~ 0.1 M were strongly crystallized along the (222) orientation. The grain size of the films was found to be high for S_c ~ 0.1 M and reduced beyond this value. The films prepared at S_c ~ 0.05 M exhibited lowest microstrain and increased beyond this value of molarity. All the films showed high transmittance in the visible region and the films deposited at a concentration, S_c = 0.1 M had a transmittance of ~ 90% that decreased with the increase of S_c due to the thickness effect. The absorption coefficient was determined to be ~ 10^5 cm^{-1} above the fundamental absorption edge. From the analysis of the absorption coefficient as a function of photon energy near the band edge the width of the Urbach tail was determined that showed higher structural order for the films prepared at S_c=0.1 M. The value of refractive index increased with the increase of precursor concentration due to the increase of the film thickness. All the films showed a normal dispersion over the entire wavelength studied. A lowest resistivity of 8.92×10^{-3} Ωcm with a carrier density (n) of approximately 3.4×10^{19} cm^{-3} was observed for the films prepared at S_c = 0.1 M. A modest mobility of < 30.2 cm^2/Vs was measured in all the films. A higher value of the figure of merit, Φ = 8.2x10^{-3} Ω^{-1}, was obtained for the films prepared at S_c= 0.1 M. The highly conducting and transparent In_2O_3 films grown with a S_c ~ 0.1 M might be useful as a window layer in solar cell fabrication.

References

[1] D. S. Ginley, C. Bright, MRS Bulletin, **25,** 8 (2000).
[2] T. J. Coutts, D. L. Young, X. Le, MRS Bulletin, **25,** 61 (2000).
[3] T. Minami, S. Takata, T. Kakumu, J. Vac. Sci. Technol. A, **14**, 1689 (1996).
[4] T. Minami, T. Miyata, T. Yamamoto, J. Vac. Sci. Technol. A, **17**, 1822 (1999).
[5] F. O. Adurodija, H. Izumi, T. Ishihara, H. Yoshioka, Appl. Phys. Lett., **74**, 3059 (1999).
[6] C. S. Huang, C. S. Tao, C. H. Lee, J. Electrochem. Soc. **144**, 3556 (1997).
[7] S. P. S. Arya, H. E. Hinterman, Thin Solid Films, **193**, 841 (1990).

[8] M. M. Yoshida, E. Andrade, Thin Solid Films, **224**, 87 (1993).
[9] C. H. Chen, A. A. J. Buysman, E. M. Kelder, J. Scnoonman, Solid State Ionics, **80**, 1 (1995).
[10] V. V. Killedar, M. D. Uplane, C. D. Lokhande, C. H. Bhosale, Ind. J. Pure and Appl. Phys. **33**, 773 (1995).
[11] J. F. D. Natale, P. J. Hood, A. B. Harket, J. Appl. Phys., **66**, 5844 (1989).
[12] C. Agashe, B. R. Marathe, M. G. Takwale, V. G. Bhide, Thin Solid Films, **164**, 261 (1988).
[13] P. Prathap, Y. P. V. Subbaiah, M. Devika, K. T. R. Reddy, Mater. Chem. Phys. **100**, 375 (2006).
[14] Raccanelli and Maddalena, J. Am. Ceram. Soc., **59**, 425 (1976).
[15] C. Agashe, M. G. Takwale, V. Bhide, S. Mahamuni, S. Kulkarni, J. Appl. Phys., **70**, 7382 (1991).
[16] E. Elangovan, M. P. Singh, K. Ramamurthi, Mater. Sci. Eng. B, **113**, 143 (2004).
[17] T. Schlenker, V. Laptev, H. W. Schock, J. H. Werner, Thin Solid Films, **480**, 29 (2005).
[18] H. R. Moutinho, F. S. Hasoon, F. Abdulfotuh, L. L. Kazmerski, J. Vac. Sci. Technol. A, **13**, 2877 (1995).
[19] P. Thilakan, J. Kumar, Mater. Sci. Eng. B, **55**, 195 (1998).
[20] J. H. Lee, B. O. Park, Surf. Coat. Technol., **184**, 102 (2004).
[21] F. O. Adurodija, L. Semple, R. Bruning, Thin Solid Films, **492**, 153 (2005).
[22] H. Sieber, St. Senz, D. Hesse, Thin Solid Films, **303**, 216 (1997).
[23] B. E. Warren, X-ray Diffraction, Dover, New York (1990) p.253.
[24] T. Schlenker, V. Laptev, H. W. Schock, J. H. Werner, Thin Solid Films, **480**, 29(2005).
[25] JCPDS: Joint Committee on Powder Diffraction Standards, Powder Diffraction File, International Center for Diffraction Data, Swarthmore, PA, card 44-1087 (1997).
[26] M. Bender, N. Katsarakis, E. Gagaoudakis, E. Hourdakis, E. Douloufakis, V. Cimalla, G. Kiriakidis, J. Appl. Phys., **90**, 5382 (2001).
[27] Z. Qiao, R. Latz, D. Mergel, Thin Solid Films, **466**, 250 (2004).
[28] G. Korotcenkov, V. Brinzari, A. Cerneavschi, A. Cornet, J. Morante, A. Cabot, J. Arbiol, Sensors and Actuators B, **84**, 37 (2002).
[29] F. K. Lotgering, J. Inorg. Nucl. Chem., **9,** 113 (1959).
[30] K. D. Rogers, D. W. Lane, J. D. Painter, A. Chapman, Thin Solid Films, **466**, 97 (2004).
[31] H. Nato, T. Minami, S. Orito, S. Takata, J. Appl. Phys., **63**, 2711 (1988).
[32] M. H. Jacobs, D. W. Pashley, M. J. Stowell, Phil. Mag., **13**, 129 (1966).
[33] R. Swanepoel, Phys. E: Sci. Instrum., **16**, 1214 (1983).
[34] A. Raza, O.P. Agnihotri, B. K. Gupta, J. Phys. D: Appl. Phys, **10**, 1871 (1977).
[35] F. Urbach, Phys. Rev., **92**, 627 (1966).
[36] G. D. Cody, T. Tiedje, B, Brooks, Y. Goldstein, Phys. Rev. Lett., **47**, 1480 (1981).
[37] M. Girtan, G. Folcher, Surf. Coat. Technol. **172**, 240 (2003).
[38] E. Hanamura, Phys. Rev. B, **37,** 1273 (1988).
[39] J. D. Dow, D. Redfield, Phys. Rev. B, **5**, 594 (1972)
[40] F. O. Adurodija, L. Semple, R. Bruning, Thin Solid Films, **492,**153 (2005).
[41] B. Hunsche. M. Vergohl, H. Neuhauser, F. Klose, B. Szyszka, T. Matthee, Thin Solid Films, **392**, 184 (2001).
[42] W. L. Bragg, A. B. Pippard, Acta Crystallogr., **6**, 865 (1953).
[43] A. M. Elkorashy, Semicond. Sci. Technol., **4**, 382 (1989).
[44] K. H. Kim, J. S. Chun, Thin Solid Films **141**, 287 (1986).
[45] G. Haacke, J. Appl. Phys. **47**, 4086 (1976).

*Corresponding author: ktrkreddy@hotmail.com